OFFICE OF NAVAL RESEARCH

Contract N00014-91-J-1927

R&T Code 413v001

Technical Report No. 10

SCANNING TUNNELING MICROSCOPY OF THE ORGANIC SEMICONDUCTOR $[(\eta-C_5Me_5)_2Ru(1,4-[2_2]\text{-cyclophane})][TCNQ]_4$

by

SHULONG LI, HENRY S. WHITE, AND MICHAEL D. WARD

Prepared for Publication in the

JOURNAL OF THE AMERICAN CHEMICAL SOCIETY

University of Minnesota
Department of Chemical Engineering and Materials Science
Minneapolis, MN 55455

February 26, 1992

SECURITY CLASSIFICATION OF THIS PAGE

REPORT DOCUMENTATION PAGE

1a. REPORT SECURITY CLASSIFICATION **Unclassified**	1b RESTRICTIVE MARKINGS
2a. SECURITY CLASSIFICATION AUTHORITY	3. DISTRIBUTION / AVAILABILITY OF REPORT **Unclassified/Unlimited**
2b. DECLASSIFICATION / DOWNGRADING SCHEDULE	
4. PERFORMING ORGANIZATION REPORT NUMBER(S) **ONR Technical Report 10**	5. MONITORING ORGANIZATION REPORT NUMBER(S)
6a. NAME OF PERFORMING ORGANIZATION **Dept of Chemical Engineering and Materials Science** 6b. OFFICE SYMBOL (*If applicable*) **Code 1113**	7a. NAME OF MONITORING ORGANIZATION **Office of Naval Research**
6c. ADDRESS (*City, State, and ZIP Code*) **University of Minnesota Minneapolis, MN 55455**	7b. ADDRESS (*City, State, and ZIP Code*) **800 North Quincy Street Arlington, VA 22217**
8a. NAME OF FUNDING / SPONSORING ORGANIZATION **Office of Naval Research** 8b. OFFICE SYMBOL (*If applicable*)	9. PROCUREMENT INSTRUMENT IDENTIFICATION NUMBER Contract No. N00014 91-J-1927
8c. ADDRESS (*City, State, and ZIP Code*) **800 North Quincy Street Arlington, VA 22217-5000**	10. SOURCE OF FUNDING NUMBERS PROGRAM ELEMENT NO. / PROJECT NO. / TASK NO. / WORK UNIT ACCESSION NO

11. TITLE (*Include Security Classification*)
Scanning Tunneling Microscopy of the Organic Semiconductor $[(\eta\text{-}C_5Me_5)_2Ru(1,4\text{-}[2_2]\text{-cyclophane})][TCNQ]_4$

12. PERSONAL AUTHOR(S)
Shulong Li, Henry S. White and Michael D. Ward

13a. TYPE OF REPORT	13b. TIME COVERED	14. DATE OF REPORT (*Year, Month, Day*)	15. PAGE COUNT
Technical	FROM 1/1/91 TO 10/31/93	February 25, 1992	

16. SUPPLEMENTARY NOTATION
submitted to the J Am Chem Soc

17 COSATI CODES			18. SUBJECT TERMS (*Continue on reverse if necessary and identify by block number*)
FIELD	GROUP	SUB-GROUP	

19. ABSTRACT (*Continue on reverse if necessary and identify by block number*)

Scanning tunneling microscopy studies of the (001) and (010) faces of the molecular semiconductor $[(\eta\text{-}C_5Me_5)_2Ru(\eta^6,\eta^6\text{-}[2_2](1,4)\text{cyclophane})]^{2+}[TCNQ]_4^{2-}$(1) are reported. The lattice constants determined from the DOS corrugation of the STM images are a = 13.8 ± 0.3Å, b = 15.9 ± 0.2Å, c = 16.6 ± 2Å, β = 88° ± 2° γ = 82° ± 2°, in good agreement with the x-ray crystal structure. STM images of both faces reveal local density of states (LDOS) associated with stacking of TCNQ molecules along the [100] direction in two crystallographically unique stacks. The tunneling current contrast conforms to the tetrameric periodicity of the TCNQ stacks observed in the crystal structure. Columnar regions of negligible tunneling current on the ac face are attributed to stacks of $(\eta\text{-}C_5Me_5)_2Ru(\eta^6,\eta^6\text{-}[2_2](1,4)\text{cyclophane})^{2+}$ dications. Each TCNQ column exhibits a tunneling current corrugation repeating at intervals of a that is attributed to tunneling into the conduction band of a antiferromagnetic $2k_F$ charge density wave (CDW) structure. The CDWs also exhibit corrugation, and antiphase modulation, at a/2 with respect to adjacent atacks, consistent with appreciable interstack Coulomb interactions (cont.)

20. DISTRIBUTION / AVAILABILITY OF ABSTRACT	21. ABSTRACT SECURITY CLASSIFICATION
☒ UNCLASSIFIED/UNLIMITED ☐ SAME AS RPT ☐ DTIC USERS	**Unclassified**
22a NAME OF RESPONSIBLE INDIVIDUAL **Henry S. White**	22b. TELEPHONE (*Include Area Code*) **(612) 625-6345** / 22c. OFFICE SYMBOL

DD FORM 1473, 84 MAR 83 APR edition may be used until exhausted. All other editions are obsolete.

SECURITY CLASSIFICATION OF THIS PAGE

and contributions from the magnetic $4k_F$ structure, which based on the tight binding approximation is equivalent to the canonical description $(TCNQ)_2^{-}$-$(TCNQ)_2^{-}$. The STM data are in agreement with magnetic susceptibility and EPR studies, which indicate significant contribution of the $4k_F$ state to the electronic structure of 1. The STM provides characterization of the local electronic structure that is manifested in the bulk electronic properties of 1.

Scanning Tunneling Microscopy of the Organic Semiconductor $[(\eta\text{-}C_5Me_5)_2Ru(1,4\text{-}[2_2]\text{-cyclophane})][TCNQ]_4$

Shulong Li, Henry S. White and Michael D. Ward*

Department of Chemical Engineering and Materials Science, University of Minnesota, Amundson Hall, 421 Washington Ave. SE, Minneapolis, MN 55455

Abstract

Scanning tunneling microscopy studies of the (001) and (010) faces of the molecular semiconductor $[(\eta\text{-}C_5Me_5)_2Ru(\eta^6,\eta^6\text{-}[2_2](1,4)\text{cyclophane})]^{2+}[TCNQ]_4^{2-}$ (**1**) are reported. The lattice constants determined from the DOS corrugation of the STM images are $a = 13.8 \pm 0.3$ Å, $b = 15.9 \pm 0.2$ Å, $c = 16.6 \pm 2$ Å, $\beta = 88^o \pm 2^o$ $\gamma = 82^o \pm 2^o$, in good agreement with the x-ray crystal structure. STM images of both faces reveal local density of states (LDOS) associated with stacking of TCNQ molecules along the [100] direction in two crystallographically unique stacks. The tunneling current contrast conforms to the tetrameric periodicity of the TCNQ stacks observed in the crystal structure. Columnar regions of negligible tunneling current on the *ac* face are attributed to stacks of $(\eta\text{-}C_5Me_5)_2Ru(\eta^6,\eta^6\text{-}[2_2](1,4)\text{cyclophane})^{2+}$ dications. Each TCNQ column exhibits a tunneling current corrugation repeating at intervals of *a* that is attributed to tunneling into the conduction band of a antiferromagnetic $2k_F$ charge density wave (CDW) structure. The CDWs also exhibit corrugation, and antiphase modulation, at *a*/2 with respect to adjacent stacks, consistent with appreciable interstack Coulomb interactions and contributions from the magnetic $4k_F$ structure, which based on the tight binding approximation is equivalent to the canonical description $(TCNQ)_2^{-}(TCNQ)_2^{-}$. The STM data are in agreement with magnetic susceptibility and EPR studies, which indicate significant contribution of the $4k_F$ state to the electronic structure of **1**. The STM therefore provides characterization of the local electronic structure that is manifested in the bulk electronic properties of **1**.

---

*Author to whom correspondence should be addressed

Introduction

Crystalline solids based on molecular components exhibit numerous electronic phenomena, including electrical conductivity, superconductivity, non-linear optical behavior and ferromagnetism.[1] The most extensively examined molecular crystals have been the low-dimensional conductors and semiconductors, which generally exhibit anisotropic conductivity along axes containing stacks of open-shell charge transfer molecules that are responsible for the formation of extended band structure. Most notable among these are the organic superconductors,[2] and more recently, ferromagnetic materials based on metallocene salts of polycyanoanions.[3] The observation of conductivity and magnetism in extended solids, particularly numerous charge-transfer salts of tetracyanoquinodimethane (TCNQ),[4] suggests a significant role for these salts in materials research. The principle advantage of molecular materials is the ability to rationally control bulk properties through molecular design. Further advances in this area, however, require a thorough understanding of the relationship between molecular structure, supramolecular structure and electronic properties. There also is a need to understand the role of *surface* topographical and electronic structure in the electrochemical crystal growth process[5] that typically is used for synthesis of these materials in order to control crystal size, morphology, growth orientation and defect density.

Recently, we reported the design and synthesis of $[(\eta\text{-}C_5Me_5)_2Ru(\eta^6,\eta^6\text{-}[2_2](1,4)\text{cyclophane})]^{2+}[TCNQ]_4^{2-}$ (**1**), which exhibited semiconducting behavior with a room temperature conductivity of ca. 1 $\Omega^{-1}cm^{-1}$.[6] Single crystal X-ray structural analysis revealed stacks of TCNQ molecules parallel to the long axes of linear $(\eta\text{-}C_5Me_5)_2Ru(\eta^6,\eta^6\text{-}[2_2](1,4)\text{cyclophane})^{2+}$ dications. This motif was attributed to structural enforcement provided by electrostatic attraction between the oppositely charged ions. The stoichiometry of **1** indicated an average charge of 0.5- per TCNQ molecule ($\rho = 0.5$, where ρ = average number of carriers on each TCNQ site), equivalent to a 1/4-filled band for a metallic state. The structure, however, revealed tetrameric periodicity in *two crystallographically unique TCNQ stacks*, suggesting charge

localization in the stacks as $(TCNQ)_4^{2-}$. One of these stacks comprised prominent $TCNQ_4$ tetramers separated by a 3.55 Å spacing, while the other exhibited more uniform interplanar spacing. Tetramerization of this $\rho = 0.5$ salt is consistent with a $2k_F$ insulating spin-Peierls structure ($2k_F = \rho/2a$; a = lattice vector), although the actual transition to this structure could not be observed since it evidently occurs at temperatures greater than room temperature. The driving force for the observed lattice distortion may arise from either a lowering of the electron kinetic energy (band energy) according to a classical Peierls distortion or a lowering of the Coulomb energy by formation of charge density waves (CDWs) as with a Wigner crystal.[7]

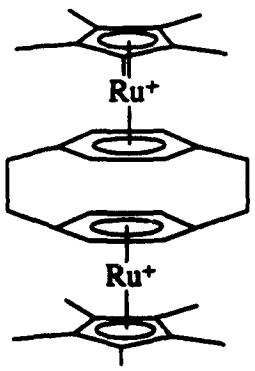

$(\eta\text{-}C_5Me_5)_2Ru(\eta^6,\eta^6\text{-}[2_2](1,4)cyclophane)^{2+}$

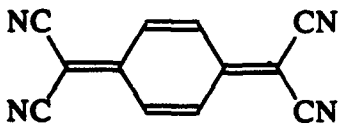

TCNQ

Magnetic susceptibility and electron paramagnetic resonance (EPR) studies of **1**[8] indicated the presence of both the antiferromagnetic $2k_F$ spin-Peierls ground state and a magnetic insulating $4k_F$ excited state 0.08 eV above the ground state that was manifested in mobile triplet excitons. While the EPR studies indicated a 7.5 Å average separation between the coupled electrons of the triplet, we were not able to elucidate *microscopic* details of the electronic and magnetic behavior such as the contribution of the different TCNQ stacks to the observed behaviors.[9] We therefore were prompted to examine the microscopic electronic structure of **1** with scanning tunneling microscopy (STM).[10] The tunneling current, i_T, measured in STM is proportional to the density of states (DOS), or $\rho(r,E_F)$, at a position r above the surface and at the Fermi energy, E_F.[11,12] The tunneling current observed on the crystal faces of **1** therefore will depend on the molecular

corrugation *and* local density of states (LDOS) of the molecular constituents in the crystal plane. Of particular interest is whether STM images of **1** (and other molecular crystals) can be interpreted on the basis of the tight-binding approximation,[13] in which the states near the Fermi energy comprise linear combinations of the highest occupied molecular orbital (HOMO) or the lowest unoccupied molecular orbital (LUMO) on the constituent molecules, and whether the tunneling current can be correlated with the bulk electronic structure.

Recently, STM has been used to examine several low-dimensional inorganic conductors[14] and superconductors,[15] as well as organic charge-transfer salts based on bis(ethylenedithiotetrathiafulvalene),[16] tetramethyltetraselenafulvalene,[17] tetrathiafulvalenium and tetracyanoquinodimethane.[18,19] Low-temperature tunneling spectroscopy[20] of organic superconductors, including point-contact studies, to determine the BCS superconducting gap also has been examined with STM.[21] We describe herein STM investigations of **1** that clearly reveal the presence of one-dimensional commensurate charge density waves (CDWs) on two different crystal faces associated with periodic charge localization within the TCNQ stacks. In addition, the contrast of the tunneling current is consistent with contribution from the $4k_F$ structure as well as the $2k_F$ CDW that is evident in the crystal structure. The amplitude of the CDWs of the two crystallographically unique stacks exhibit an anti-phase modulation due to Coulomb correlations between the TCNQ stacks. The results suggest that Coulombic interactions play an important role in the crystal and electronic structure of **1**. These studies indicate clearly the value of STM in elucidating the electronic structure of these materials on a molecular level.

Experimental

Crystals of **1** were grown by electrochemical reduction of TCNQ (0.20 mmol) on Pt electrodes at 0.30 V (vs. SCE) in the presence of $(\eta\text{-}C_5Me_5)_2Ru(1,4\text{-}2_2\text{-cyclophane})^{2+}$ (0.045 mmol) in 0.1 M $n\text{-}Bu_4N^+BF_4^-$/nitromethane as described previously.[6] After several days, large black parallelipiped crystals were obtained on the electrode surface. The crystals exhibited the morphology depicted in Figure 1, with typical crystal dimensions of 4 x 2 x 0.5 mm. The

morphological indices of crystal faces of **1** decreased in the order (001) > (010) > (100) > (111). All crystals were used as grown, and no additional cleaning or preparation was performed.

A Nanoscope II ™ scanning tunneling microscope with either mechanically cut 80% Pt/20% Ir or 70% Pt/30% Rh tips was used to obtain images. Crystals were mounted with adhesive tape onto an conductive aluminum substrate attached to the STM fixture. Bias voltages ranging from -600 to -1400 mV (tip vs. sample) generally could be employed with setpoint currents ranging from 0.10 - 0.30 nA. Images were obtained on the (001) and (010) faces and attempts to examine the (100) face were unsuccessful. Lateral dimensions (x,y) observed in the STM images were calibrated with a graphite standard. Images could be obtained in either constant current or constant height mode, but all images shown here were obtained in the constant height mode owing to the better quality of data obtained. Extended Huckel calcuations were performed at the STO-3G level using a Tetronix CACHE molecular modeling workstation.

Results and Discussion

Crystal structure of 1 and crystal plane topography. Elucidation of the dependence of the tunneling current on the tip distance from LDOS requires understanding of the molecular topography of the crystal plane under examination. The single crystal X-ray structure of **1**, which crystallizes in the $P\bar{1}$ space group (Table 1), reveals stacks of dications along the *a* axis, with adjacent TCNQ stacks nearly parallel to dication stacks (Figure 1). This results in "sheets" of cations and anions in the *ab* (001) plane that alternate along the [001] direction. Notably, two crystallographically distinct TCNQ stacks are evident, one exhibits a strong tetamerization with a 3.55 Å separation between tetramers (labelled A in Figures 1 and 2). The other (B) exhibits more uniform spacing between TCNQ planes, although a tetrameric repeat motif is still evident. Stack A exhibits a much larger molecular corrugation normal to the stacking *a* axis as determined from the relative heights of the methylidene carbon atoms normal to the stacking axis (Figure 2, bottom). Assuming a similar density of electronic states on each TCNQ molecule, a larger corrugation of the tunneling current is expected for stack A than for stack B with corrugation length scales equal to

that of the tetramer length. We show below that the tunneling current contrast observed in the STM images allows us to distinguish these two crystallographically unique stacks.

The three principal crystal planes have significantly different molecular topographies. The *bc* (100) face normal to the stacking axis has rows of dication stacks and TCNQ stacks that alternate along the [001] direction. The (001) face may be terminated with either sheets of cations or anions, although in order to maintain elecroneutrality the (001) and (00$\bar{1}$) faces overall must have equal numbers of dications and $[TCNQ]_4^{2-}$ species. The (001) plane is depicted by the solid line at the bottom of the rightmost panel in Figure 1, this plane projecting normal to the plane of the paper. When the (001) face is terminated with anions, it contains both crystallographically unique TCNQ stacks alternating ...ABAB... along the [010] direction. The *ac* (010) plane consists of alternating stacks of dication and TCNQ molecules, but the TCNQ stacks in the surface plane may be either stack A or B. The (010) plane is depicted by the solid line at the left of the right panel in Figure 1, this plane projecting normal to the plane of the paper. In Figure 1, we have depicted abitrarily this surface plane as containing stack B, with stack A in the next layer.

[Figure 1]

[Figure 2]

Electronic structure. The electronic structure of **1** can be described on the basis of extended linear chains of $\rho = 0.5$ TCNQ sites (ρ = the average charge per site) with electronic band structures based on linear combinations of lowest unoccupied molecular orbitals (LUMOs) of TCNQ. Extended Huckel calculations indicate that the TCNQ LUMO consists largely of contributions from the exocyclic methylidene carbon atoms with lesser contributions from the nitrogen and ring carbon atoms.[22] Since the TCNQ LUMO is partially occupied in **1**, the corresponding bands derived from these orbitals are likely to be those nearest E_F. The dications, however, are closed shell species with an 18-electron configuration, and therefore are not likely to possess states in the vicinity of E_F. This is supported by comparison of the electrochemical redox

potentials of these two species ($E^{o}_{TCNQ/TCNQ^-}$ = +0.19 V vs. SCE in acetonitrile whereas the dication is not oxidized or reduced within the solvent limits of -2.0 to +2.0 V vs. SCE). Interpretation of the STM images therefore is best described in terms of available states on the TCNQ stacks.

The semiconducting properties and crystal structure of **1** suggests that the local electronic structure plays an important role in the properties of **1**. A tight-binding approximation based upon a linear combination of the TCNQ LUMOs in the tetramers therefore provides a valid description of the band structure associated with the extended TCNQ stacks. Each $(TCNQ)_4^{2-}$ tetramer comprises four TCNQ LUMOs whose linear combinations provide four new wavefunctions Ψ_1 - Ψ_4 (Figure 3,left). If the spin pairing energy (U) is small compared to the Huckel overlap integral (β), Ψ_1 will be completely filled. Conversely, when U>β, significant population of Ψ_2 can result.

[Figure 3]

The tight-binding band approximation incorporates the localized states Ψ_1 - Ψ_4 into extended states (Figure 3,right). When U<4t (t = the transfer integral, the tight-binding equivalent of β) a ρ = 0.5 system can adopt a metallic band structure in which the band is 1/4-filled. The lower portion of the band is predominantly bonding in character and the upper portion antibonding, reflecting the range of energy from Ψ_1 to Ψ_4. The dispersion of states arises from the various linear combinations of Ψ_1 - Ψ_4. If the Coulomb repulsion energy (U) is large, a high-spin state can result (U is the tight-binding equivalent of the spin pairing energy described above). The energy of this state can be further lowered by formation of a magnetic $4k_F$ structure which results in dimerization of the one-dimensional stacks, lowering of the electron kinetic energy and formation of a band gap. Further lattice distortion to a tetamerized stack and formation of a diamagnetic $2k_F$ structure can occur if the energetic cost of the lattice distortion can be compensated by the additional lowering of the electron kinetic energy or favorable changes in Coulombic terms. Comparison of the localized and tight-binding band descriptions of the $2k_F$ structure gives valence

and conduction bands consisting of states based on Ψ_1 and Ψ_2 states, respectively. In this case, U is less than the energy gap between the valence and conduction bands. In contrast, the valence band of the $4k_F$ structure consists of states based on both Ψ_1 and Ψ_2. The upper band would comprise states based on Ψ_3 and Ψ_4, with the former dominating at the bottom of the band. The $4k_F$ structure is favored when U is large, synonymous with a large spin pairing energy in Ψ_1.

The crystal structure, magnetic susceptibility and EPR studies of **1** indicate that at room temperature the electronic structure is dominated by the antiferromagnetic $2k_F$ structure which is equivalent to a filled Ψ_1 state in the local description. *This suggests that electron tunneling from the tip to 1 would primarily involve states in a conduction band based on* Ψ_2. The bottom of this band consists of in-phase linear combinations of Ψ_2 (Figure 3,center). Magnetic susceptibility and EPR studies indicated, however, the presence of a high-spin triplet excitonic state corresponding to an approximately 5% contribution of the $4k_F$ structure ($\Psi_1 + \Psi_2$) states at room temperature. Participation of the $4k_F$ state is expected to affect the electron tunneling characteristics in that tunneling would involve higher Ψ_2 states, which correspond to out-of-phase linear combinations of Ψ_2. Alternatively, states in the lower portion of the Ψ_3 band derived from in-phase combinations of Ψ_3 may play a role if the $4k_F$ structure is present. The phase relationships of the linear combinations of the higher Ψ_2 states and the lower Ψ_3 states provide nodal planes at $a/2$, the node density increasing with increasing energy. Filling of the Ψ_2 states also corresponds to a shift of charge density towards the ends of the $(TCNQ)_4^{2-}$ tetramer at the expense of the center, in accord with the canonical description $(TCNQ)_2^{-}(TCNQ)_2^{-}$ assigned to the coupled electrons of the triplet species in our previous EPR studies. This canonical description implies dimerization of the TCNQ stacks as expected for the $4k_F$ structure.

STM images. The morphology of crystals of **1** results in large flat faces normal to all three principle directions that are adequate for locating the STM tip on all three principal faces. High quality images of the (001) and (010) faces were readily acquired. We were not successful, however, in obtaining interpretable images of the (100) face, which is normal to the stacking axis. In addition, high quality images of the (001) and (010) faces could only be obtained using a

negative tip bias (-600 to -1400 mV) and low setpoint currents (0.10 - 0.30 nA). All attempts to obtain images with a positive tip bias were complicated by an apparent high resistivity which made tip engagement difficult. We attribute this behavior to the semiconducting properties of **1**, as metallic organic conductors generally afford images that are independent of polarity.[23]

STM images of the (001) face of **1** (Figure 4) displayed large molecularly smooth regions. No structures were observed that might signify transitions between anion and cation covered regions of the (001) plane or monomolecular steps. The image of the (001) face revealed a periodic corrugation of tunneling current along two directions forming an angle of $82^{o} \pm 2^{o}$, nearly identical to the value of γ determined in the X-ray structure analysis. The tunneling current features repeat along these directions at intervals of 13.8 ± 0.3 Å and 15.9 ± 0.2 Å, equivalent to the crystallographic unit cell lengths along the *a* and *b* axes, respectively (Table 1). Notably, two distinct columns with different corrugation patterns are evident, the colums separated by slightly less than *b*/2. We attribute this observation to the known presence of two crystallographically distinct TCNQ stacks. The size of the features in each column correspond to that expected for the $(TCNQ)_4^{2-}$ tetramers exposed on this face, strongly suggesting that the observed tunneling current reflects a significant localization of state density on these entities (the rectangular boxes in Figure 4 serve as a visual aid for illustrating the tetrameric periodicity). Further examination of the STM image reveals that the tunneling current contrast is significantly larger in one of the columns (column A in Figure 4). This column therefore is assigned to the strongly tetramerized stack A (Figure 2) whose tetramers have greater inclination with respect to the (001) plane (vide supra). This assignment, however, is not definitive as it assumes a uniform density of states within the tetrameric unit. There is no evidence of significant state density *between* stacks. The lack of states between stacks is consistent with a small transfer integral and small bandwidth perpendicular to the stacking direction, factors that favor formation of the $2k_F$ structure.

[Figure 4]

Closer inspection of the (001) face and analysis of the corresponding line profiles also reveals a secondary corrugation in the DOS contrast in each column at 6.3 Å intervals, corresponding to $a/2$. Fourier-filtered images (Figure 4b) clearly show that the primary features have a "dumbell" shape, suggesting further localization of the DOS within the $(TCNQ)_4^{2-}$ tetramers. The crystal structure of **1** (Figures 1, 2) does not reveal a *topographical* basis for this observation. That is, there is no severe molecular corrugation at $a/2$ that could account for the diminished tunneling current at $a/2$, suggesting that *modulation of the electron state density* in the TCNQ stacks is responsible for this tunneling behavior. It is also evident that the tunneling current maxima in adjacent columns are out-of-phase with respect to the [010] direction as depicted in Figure 4.

STM images of the (010) face (Figure 5) exhibit two columns separated by 6.5 Å with different tunneling current corrugation, with a corrugation repeat distance within each column of 13.8 ± 0.3 Å, in agreement with the lattice parameter a determined from the crystal structure. The magnitude of the tunneling current is similar for the two columns. The periodicity between pairs of these columns is 16.6 ± 0.2 Å, equivalent to the c lattice parameter. The angle between these two directions is $88^o \pm 2^o$, in good agreement with β determined from the crystal structure. The lattice parameters therefore are consistent with the molecular motif of the (010) plane, which consists of parallel stacks of anions and dications. The tunneling current maxima in adjacent columns are out-of-phase with respect to the [001] direction, identical to the behavior observed on the (001) face. The wide region of negligible tunneling current separating the pairs of columns is consistent with the stacks of the insulating closed shell dications which are not likely to have states near E_F. Unlike the (001) face, a corrugation with a length scale of $a/2$ was not evident in STM images of the (010) face.

Although we were not able to detect monomolecular steps, line defects were occasionally found in the STM images of the (010) face. The line dislocation in Figure 6 is approximately 10 Å wide and is rather abrupt, clearly showing the interruption of the columns of tunneling current. The nearly identical height of the average surface plane on each side of the line dislocation suggests

that the defect represents a missing row of molecules rather than a step. The direction of the dislocation is roughly along the [401] direction and the mechanism for the formation of the dislocation is not understood at this time.

[Figure 5]

[Figure 6]

The observation of two separate columns of tunneling current on the (010) face suggests tunneling into the two crystallographically distinct TCNQ stacks, similar to the behavior observed on the (001) face. This is rather surprising, however, because only one of the crystallographically unique TCNQ stacks is exposed on the (010) surface plane. One of the exocyclic $=C(CN)_2$ groups of each TCNQ molecule in the surface stack protrudes from the surface plane, while the other is nestled behind the surface dications. Based on the crystal structure, the average separation between the surface stack and the one immediately beneath the surface plane is 7.7 Å, much larger than that suggested by the tunneling current for the two columns. In addition, the *resolved* distance in the (010) plane along the [001] direction between the surface TCNQ stack and the stack immediately beneath the surface plane is only 3 Å, much less than the 6.5 Å separating the columns of tunneling current.[24] While the tunneling mechanism is not well understood, we attribute the apparently enhanced tunneling to the submerged TCNQ stack to mediation by the dication stacks. It is plausible that the positive charge of the dication stacks screens the charge of the submerged TCNQ stack, resulting in an increase in the potential drop between the tip and this region and a corresponding increase in the tunneling rate.

Relationship of LDOS and charge density waves. The tunneling current contrast periodicity of a on the (001) face is consistent with the phase relationships expected for tunneling into the lower portion of the conduction band of the $2k_F$ structure, which consists of states based on in-phase combinations of Ψ_2 (Figure 3). The secondary alternation at $a/2$, however, suggests

participation of states in the upper portion of the conduction band of the $2k_F$ structure, which consists of states based on out-of-phase combinations of Ψ_2. Alternatively, tunneling at $a/2$ intervals can be viewed as tunneling into the lower portion of the upper band in the $4k_F$ structure, which consists of states based on in-phase combinations of Ψ_3 (note that the in-phase linear combinations of Ψ_3 are identical to the out-of-phase combinations of Ψ_2). In either case, the increase in nodal density at $a/2$ relative to states derived from linear combinations of Ψ_1 or the lower portion of the Ψ_2 band is expected to give tunneling features tending toward those observed on the (001) face. Although the crystal structure of **1** strongly implicates the $2k_F$ tetramerized structure, these STM results clearly indicate the $4k_F$ contribution to the electronic structure of **1**, in accord with our previous magnetic susceptibility and EPR measurements which established a roughly 5% contribution from the $4k_F$ structure at room temperature.

The absence of tunneling current corrugation at $a/2$ on the (010) face may indicate that images of this face reflect tunneling into states different than those involved in tunneling on the (010) face, for example states with greater contribution from higher levels of Ψ_3 or possibly lower levels of Ψ_2 where nodal structure at $a/2$ is absent (Figure 3). However, the stacks imaged on the (010) face are crystallographically identical to those on the (001) face. Images of the (010) face were more difficult to obtain and generally were of poorer quality than the (001) face, which we attributed to the apparent lower conductivity of the (010) face. Accordingly, the absence of the $a/2$ alternation in images of the (010) face may be an artifact of this reduced conductivity .

The localization of state density evident from the tunneling current corrugation in the STM images can be described reasonably as charge-density waves (CDWs), mixed waves of charge density modulation and periodic lattice distortion. Previous STM studies have noted CDWs on two-dimensional materials inorganic solids such as TaS_2 and WSe_2.[8,9] To our knowledge, this is the first observation by STM of CDWs and the accompanying anti-phase modulation on the surface of a molecular organic solid. Since the periodicity of the tunneling current and the crystallographic lattice parameters are equivalent, the observed DOS represent a commensurate CDW.[25] Unlike incommensurate CDWs that can "slide" along a lattice vector and provide a mechanism for high

conductivity, commensurate CDWs are pinned on lattice sites at regular intervals, accounting for the semiconducting properties of **1**. There are two distinct one-dimensional CDWs in adjacent columns that are distinguished by different tunneling current contrast. The images obtained on the (001) and (010) faces are representations of the same pair of one-dimensional CDWs probed from near orthogonal directions.

Particularly noteworthy is the *anti-phase modulation of tunneling current that is evident in the STM images of 1*. The charge localization implicit in the CDWs can result from substantial interstack Coulomb repulsions between stacks which can be minimized by modulation of the charge density between stacks at intervals corresponding to the charge alternation. This modulation also must reflect a corresponding perturbation of the state density in order to accomodate the redistribution of charge in the tetrameric stacks. That is, $\Psi_1 - \Psi_4$ must be polarized so that the amplitude of these wavefunctions with respect to adjacent stacks is also out-of-phase. The anti-phase modulation also is evident on the (010) face, although the modulation primarily conforms to intervals of *a* rather than *a*/2 as described above

Anti-phase modulation of one-dimensional CDWs has been noted for other low-dimensional solids based on diffuse X-ray scattering studies,[26] with three-dimensional ordering of CDWs experimentally observed below the Peierls transition temperature.[27] The observation of this modulation between the one-dimensional CDWs on both faces confirms that these images are representations of the same pairs of CDWs, and also corroborates the assignment of one of the CDWs on the (010) face to the TCNQ stack beneath the surface plane. The CDWs can be described by $q_i = q_o \cos\Phi_i$, where q_i is the amplitude of the CDW and Φ_i the phase angle of the i^{th} CDW with respect to a reference. The Coulomb interaction energy between two stacks is given approximately by equation (1), in which $\varepsilon_\perp$ is the perpendicular static dielectric constant, $\kappa_o(x)$ the complete elliptic integral of the first kind[28] and $d_{s\text{-}s}^{[hkl]}$ the distance between TCNQ stacks along the [hkl] direction (Figure 7).[29] Therefore, adjacent CDWs that are 90° out of phase will represent the minimum Coulombic energy. This modulation is depicted schematically in Figure 7, where

$d_{s\text{-}s}[010]$ and $d_{s\text{-}s}[001]$ represent the distance between the stacks along the *b* and *c* directions, respectively. The Coulomb energy will also be affected by interactions between stacks along the [021] and [$0\bar{2}1$] directions, although these will be less significant than those along the [010] direction.

$$U_{s\text{-}s}[hkl] = (4\varepsilon_\perp)^{-1} q_o^2 [2\kappa_o(2k_F d_{s\text{-}s}[hkl])]\cos(\Phi_i - \Phi_j) \qquad (1)$$

[Figure 7]

Based on the crystal structure, we expect that $U_{s\text{-}s}[010] > U_{s\text{-}s}[001] > U_{s\text{-}s}[021] > U_{s\text{-}s}[0\bar{2}1]$ because $d_{s\text{-}s}[010]$ (on the *ab* face) represents the smallest interstack contact. Coulomb interactions between stacks along the other directions will be smaller owing to larger values of $d_{s\text{-}s}$. For example, the interactions between stacks in the (010) plane are smaller because of larger $d_{s\text{-}s}$ ($d_{s\text{-}s}[001] = c$) and the presence of interleaving dication stacks that are expected to have a relatively large value of $\varepsilon_\perp$. This is evident from the STM images: adjacent stacks on the (001) plane are anti-phase modulated along the [010] direction, whereas the stacks on the (010) face separated by the dications are in phase along the [001] direction.

On a molecular level, the tunneling current corrugation at *a*/2 observed on the (001) face can be attributed to contributions from the canonical form $(TCNQ)_2^{-}(TCNQ)_2^{-}$ of the $4k_F$ structure. The charge is partially localized on the $(TCNQ)_2^{-}$ dimers in an alternating manner so as to reduce charge repulsion between the stacks. We note that the onset of the 3-D CDW resulting from interstack interactions occurs at a lower temperature than the 1-D CDW in other organic conductors because of shorter correlation lengths in the transverse direction owing to reduction of the interstack Coulomb interaction by counterions. In the case of **1**, however, interactions between the TCNQ stacks along the [010] direction are not mediated by cations, and strong Coulomb correlations can be expected.

The observation of anti-phase modulated CDWs strongly suggest that Coulombic factors play an important role in the crystal and electronic structure of **1**, rather than simply a lowering of the electron kinetic energy. The proximity of the stacks and the ability to minimize the Madelung energy by anti-phase amplitude modulation lowers the energetic cost associated with the lattice distortion from the unobserved metallic state with uniform TCNQ stacks. *Significantly, the two crystallographically independent dications are also anti-phase modulated with respect to adjacent stacks* (Figure 8). Although the actual charge distribution in the dications is not known, the centroids of the $(\eta\text{-}C_5Me_5)_2Ru(\eta^6,\eta^6\text{-}[2_2](1,4)cyclophane)^{2+}$ dications are anti-phase modulated along [100] at intervals of $a/2$. This strongly suggests that Coulombic *attractive* forces between the localized charges of the CDW and the dication also contribute to the observed electronic structure. That is, the dications likely play an important role in pinning the CDW in a commensurate manner.

[Figure 8]

The crystal structure of **1** therefore is a manifestation of several energetic terms, including van der Waals forces associated with close packing, π–π overlap between TCNQ molecules in each stack, electronic interactions between stacks (albeit negligible) and Coulombic interactions associated with the ionic charges. The Coulombic interactions induce charge localization, thereby stabilizing the magnetic $4k_F$ $(TCNQ)_2^-(TCNQ)_2^-$ state that is manifested as EPR-observable triplet excitons. The formation of triplet excitons would not be possible if $U<4t$ and the ground state of **1** was metallic. The anti-phase modulation and the accompanying reduction in total free energy therefore facilitates formation of the high spin triplet state by condensation of charge on the $(TCNQ)_2^-$ dimers.

The STM images of the (001) face provide some indication of the differences in the electronic properties of the two crystallographically unique TCNQ stacks. The crystal structure indicates that stack B has more uniform interplanar spacing (i.e. larger bandwidth) than stack A but a smaller topographical corrugation along the stacking axis (Figure 2). Notably, the apparent

height corrugation is greater in the column denoted A in Figure 4. This column also exhibits less continuity of tunneling current along the stacking axis compared to column B. These observations support the assignment of two crystallographically unique TCNQ stacks to their corresponding columns of tunneling current as denoted in Figure 4. The larger bandwidth suggested by the more significant tunneling continuity in column B is consisent with the more uniform spacing in stack B. This larger bandwidth may suggest that column B is responsible for the $4k_F$ magnetic state, but the STM studies do not allow a definitive assignment of the triplet species. The intervals of tunneling current amplitude ($a/2$ = 6.9 Å) are similar to the 7.5 Å value determined by EPR for the average separation between coupled electrons. We note that the STM data also suggest a 7.8 Å separation between tunneling current maxima on adjacent stacks. This may suggest that the coupled electrons of the triplet exciton may be located on adjacent stacks. Although very weak interchain coupling between spins (< 0.001 eV) has been suggested for the triplet excitons of $MEM(TCNQ)_2$[30] (MEM = N-methyl N-ethylmorpholinium), this is not likely in **1** given the large spin exchange coupling (0.08 eV) and our previous single crystal EPR studies of **1**[8] that indicated that the major triplet species was coincident with the TCNQ stacking axes.

Relationship of LDOS to electrochemical crystal growth. The ability to obtain clear images of different crystal planes can, in principle, provide insight into the electrocrystallization process. Synthesis of low-dimensional conductors typically is accomplished by electrocrystallization methods in which an acceptor (donor) species is reduced (oxidized) at the surface of the growing conductive crystal. Subsequent condensation of the reduced (oxidized) species with the counterions and attachment of molecular aggregates to the crystal results in growth. The factors that control the morphology of electrochemically grown crystals, which typically tend to grow as anisotropic needles with a clearly defined preference for growth along the stacking axis, are of particular interest. The morphology of crystals depends upon the relative rates of growth along different directions, which in turn will depend upon the electron transfer rate and the rate of attachment of molecules or their aggregates to the different crystal faces. The observation of tunneling current on the both the (001) and (010) planes indicates that electron

transfer to TCNQ molecules at these faces is feasible and can account for the crystal growth on both faces. While there appears to be a greater DOS on the (001) face, growth on this face was slower than on the (010) face. It is important to note that the (001) face imaged in our studies likely was terminated with an anion layer; other regions of the crystal will necessarily be covered with cation layers in order to maintain electroneutrality. Accordingly, growth along the [001] direction must proceed by alternating attachment of layers of TCNQ anions and $(\eta\text{-}C_5Me_5)_2Ru(\eta^6,\eta^6\text{-}[2_2](1,4)cyclophane)^{2+}$ dications. If the dications inhibit electron transfer and subsequent growth along this direction, crystal growth along the [001] direction will be diminished even though substantial DOS were observed on on the (001) face. In contrast, the DOS on the (010) face will be constant during crystal growth. Clearly, the interpretation of crystal morphology based on presumed relationships between DOS and electron transfer rates must necessarily take into account the details of the crystal structure.

Conclusions

The results described above clearly show that STM can provide highly resolved images of the crystal planes of molecular organic conductors which can be correlated with the electronic structure and molecular topology of crystal faces. Significant tunneling current is observed on two different crystal planes of **1** that can be assigned to tunneling into the conduction band of commensurate CDW structures based on contributions from the $4k_F$ excited state in addition to the $2k_F$ ground state. Tunneling current between the one-dimensional CDWs is negligible, reflecting a lack of state density between TCNQ anion stacks that is consistent with the low-dimensional nature and semiconducting properties of **1**. The observed anti-phase modulation of the CDWs results from strong Coulomb repulsion between two crystallographically unique TCNQ anion stacks and Coulomb attraction between the TCNQ anion stacks $(\eta\text{-}C_5Me_5)_2Ru(\eta^6,\eta^6\text{-}[2_2](1,4)cyclophane)^{2+}$ cations. The STM therefore has provided a detailed, molecular level characterization of the DOS on different crystal planes that reflects the bulk electronic properties of **1**. These STM data clearly show the charge localization responsible for the semiconducting properties of this material and the

mobile triplet excitons observed in its EPR spectrum. These studies demonstrate that STM can play an important role in the characterization of low-dimensional solids, providing insight into their electronic structure. We also anticipate that the detailed characterization of the surface topography and electronic structure provided by the STM will advance understanding of electrochemical crystal growth mechanisms, and may provide a basis for nanoscale STM assisted synthesis on single crystals of these materials.

Acknowledgments

The support of the National Science Foundation (NSF/DMR-9107179), the Office of Naval Research and the NSF Center for Interfacial Engineering (NSF Engineering Research Centers Program, CDR 8721551) is gratefully acknowledged.

Table I. Lattice constants for $[(\eta\text{-}C_5Me_5)_2Ru(\eta^6,\eta^6\text{-}[2_2](1,4)\text{cyclophane})][TCNQ]_4$ as determined from X-ray diffraction and STM.[a]

Method	a (Å)	b(Å)	c(Å)	α	β	γ
X-ray	13.963	16.107	16.855	67.60	87.30	81.41
STM	13.8±0.3	15.9±0.2	16.6±0.2	b	88±2	82±2

[a] uncertainty in lattice constants determined by STM represents 2σ. [b]a could not be measured since the *ab* face was not investigated

Figure Captions

Figure 1. View of **1** normal to the *ab* , *ac* and the *bc* faces. STM tips on the right panel are drawn as a visual aid to illustrate the scanning direction on the *ac* and *ab* planes, which are normal to the plane of the paper. The *ab* face is depicted here as terminated with both crystallographically unique TCNQ anion stacks, repeating ...ABAB... along the [010] direction. The *ac* face, which has alternating TCNQ anion and $(\eta\text{-}C_5Me_5)_2Ru(\eta^6,\eta^6\text{-}[2_2](1,4)cyclophane)^{2+}$ dication stacks, is depicted with TCNQ stack B (see Figure 2) on the surface plane and stack A in the layer immediately below. The crystal morphology of **1** is depicted with the Miller indices of the faces identified.

Figure 2. Segments of the two crystallographically independent TCNQ stacks of **1** as viewed along the [010] direction. Stack A is strongly tetramerized with the tetramers separated by 3.55 Å and stack B has more uniform interplanar spacings. The interplanar spacings are indicated above each stack. The line profiles indicate the relative heights along the *a* axis of the TCNQ methylidene carbon atoms exposed on the *ab* face.

Figure 3. Schematic representation of the Ψ_1 - Ψ_4 linear combinations of TCNQ LUMOs in the $(TCNQ)_4^{2-}$ tetramer (left), octameric segments of the linear combinations of Ψ_1 - Ψ_4 (center), and bands according to the tight-binding approximation based on these combinations (right). The filled levels of the $2k_F$ and $4k_F$ states correspond to linear combinations of Ψ_1 and $(\Psi_1 + \Psi_2)$, respectively. The lowest and highest states of each band of the $2k_F$ structures are shown. For purposes of clarity only the dominant wavefunctions on the exocyclic methylidene carbon atoms are shown. Each TCNQ LUMO is partially filled ($\rho = 0.5$). The nodal planes, indicated by the solid lines, portray the patterns of nodes in the higher Ψ_2 states and lower Ψ_3 states that are believed to correspond to the tunneling current contrast at *a*/2.

Figure 4. STM images of the *ab* (001) face of **1**: (a) raw data, (b) after Fourier filtering. The rectangular boxes are included as a visual aid to depict the putative tetrameric repeat unit in the two crystallographically independent stacks. The 90° anti-phase modulation between adjacent stacks is illustrated, the amplitude scaling approximately with the tunneling current. Tunneling conditions: tip bias = -651 mV, setpoint current = 0.21 nA. Maximum contrast of tunneling current corresponds to 10 Å.

Figure 5. STM images of the *ac* (010) face of **1**: (a) raw data, (b) after Fourier filtering. The rectangular boxes are included as a visual aid to depict the putative tetrameric repeat unit in the two crystallographically independent stacks. The 90° anti-phase modulation between adjacent stacks is illustrated, the amplitude scaling approximately with the tunneling current. Tunneling conditions: tip bias = -1100 mV, setpoint current = 0.09 nA. Maximum contrast of tunneling current corresponds to 20 Å in (a) and 12 Å in (b).

Figure 6. STM image of the *ac* (010) face of **1** depicting a line defect. Tunneling conditions: tip bias = -1100 mV, setpoint current = 0.09 nA. Maximum contrast of tunneling current corresponds to 12 Å.

Figure 7. Schematic representation of the anti-phase modulation between TCNQ stacks. The unshaded and shaded regions denote the absence and presence of state density. The two crystallographically independent TCNQ stacks in **1** are represented by the columns of circles and squares.

Figure 8. Position of the $(\eta\text{-}C_5Me_5)_2Ru(\eta^6,\eta^6\text{-}[2_2](1,4)cyclophane)^{2+}$ cations in **1** as viewed slightly off the [001] direction. The organic ligands have been omitted for clarity, with Ru^+ cation centers of the same molecule connected. The crystallographically unique molecules are indicated by different shading.

References

[1](a) Lehn, J.-M. *Angew. Chem. Int. Ed. Eng.* **1988**, *27*, 89. (b) *Molecular Electronic Devices*, Carter, Forrest L., Ed.; Marcel Dekker, New York, **1982**. (c) *Extended Linear Chain Compounds*, Vol 1 - 3, Miller. J.S., Ed.; Plenum, New York, **1982-1983**. (d) Desiraju, G. Crystal Engineering, Elsevier, New York, 1989. (e) Miller, J. S.; Epstein, A. J.; Reiff, W. M. *Science*, **1988**, *240*, 40.

[2](a) Williams, J. M.; Carneiro, K. *Adv. Inorg. Chem. RadioChem.*, **1985**, *29*, 249. (b) Inokuchi, H. *Angew. Chem. Int. Ed. Eng.* 1988, 27, 1747-1751. (c) Emge, T. J.; Leung, P. C. W.; Beno, M. A.; Wang, H. H.; Firestone, M. A.; Webb, K. S.; Carlson, K. D.; Williams, J. M.; Venturini, E. L.; Azevedo, L. J.; Schirber, J. E. *Mol. Cryst. Liq. Cryst.* **1986**, *132*, 363. (d) Montgomery, L. K.; Geiser, U.; Wang, H. H.; Beno, M. A.; Schultz, A. J.; Kini, A. M.; Carlson, K. D.; Williams, J. M.; Whitworth, J. R. Synth. Met. **1988**, *27*, A195.

[3](a) Miller, J. S.; Epstein, A. J.; Reiff, W. M. *Acc. Chem. Res.* **1988**, *21*, 114. (b) Miller, J. S.; Epstein, A. J.; Reiff, W. M. *Science*, **1988**, *240*, 40.

[4]Broderick, W. E.; Thompson, J. A.; Day, E. P.; Hoffman, B. M. *Science*, **1990**, *249*, 401.

[5]Ward, M. D., *Electroanalytical Chemistry* **1989**, Vol. 16, Bard, A.J., Ed.; Marcel Dekker, New York, p 181.

[6]Ward, M. D.; Fagan, P. J.; Calabrese, J. C.; Johnson, D. C. *J. Amer. Chem. Soc.* **1989**, *111*, 1719.

[7](a) Torrance, J. B. *Phys. Rev. B* **1978**, *17*, 3099-3103. (b) Torrance, J. B.; Silverman, B. D. *Phys. Rev. B* **1977**, *15*, 788.

[8]Morton, J. R.; Preston, K. F.; Ward, M. D.; Fagan, P. J. *J. Chem. Phys.* **1989**, *90*, 2148-2153.

[9]Pairs of crystallographically unique TCNQ stacks in other charge-transfer salts and their relative contribution to electronic structure, particularly magnetic properties, have been reported; for

example: (a) Oostra, S.; Visser, R. J. J.; Sawatzky, G. A.; Schwerdtfeger, C. F. *J. Phys. C.* **1983**, *44*, 1381. (b) Schwerdtfeger, C. F.; Wagner, H. J.; Sawatzky, *Solid State Comm.* **1980**, *35*, 7. (c) Visser, R. J. J.; Smaalen, S. V.; De Boer, J. L.; Vos, A. *Mol. Cryst. Liq. Cryst.* **1985**, *120*, 167. (d) Schwerdtfeger, C. F.; Oostra, S.; Sawatzky, G.A. *Phys. Rev. B.* **1982**, *25*, 1786.

[10](a) Binnig, G.; Rohrer, H.; Gerber, Ch.; Weibel, E.; *Phys. Rev. Lett.* **1982**, *49*, 57. (b) Spong, J. K.; Mizes, H. A.; LaComb, L. J.; Dovek, M. M.; Frommer, J. E.; Foster, J. S. *Nature*, **1989**, *338*, 137. (c) Smith, D. P. E.; Horber, H.; Gerber, Ch.; Binnig, G. *Science*, **1989**, *245*, 43.

[10]Binnig, G.; Quate, C. F.; Gerber, Ch. *Phys. Rev. Lett.* **1986**, *56*, 930.

[11](a) Tersoff, J.; Hamann, D. R. *Phys. Rev. B* **1985**, *31*, 805-813. (b) Tersoff, J. *Phys. Rev. Lett.* **1986**, *57*, 440.

[12](a) Tekman, E.; Cirai, S. *Phys. Rev. B* **1989**, *40*, 10 286. (b) Tromp, R. M. *J. Phys. Cond. Matter* **1989**, *1*, 10 211.

[13](a) Slater, J. C.; Koster, G. F. *Phys. Rev.* **1954**, *94*, 1498. (b) Bloch, F. *Z. Phys.* **1928**, *52*, 555. (c) Epstein, A. J.; Miller, J. S. Prog. Inorg. Chem. **198X**, *20*, 1. (d) Garito, A. F.; Heeger, A. J. *Acc. Chem. Res.* **1974**, *7*, 232-240.

[14](a) Lieber, C. M.; Wu, X. L. *Acc. Chem. Res.* **1991**, *24*, 170-177. (b) Parkinson, B. A. *J. Amer. Chem. Soc.* **1991**, *113*, 7833-7837.

[15](a) Wu, X. L.; Lieber, C. M.; Ginley, D. S.; Baughman, R. *J. Appl. Phys. Lett.* **1989**, *55*, 2129. (b) Parks, D. C.; Wang, J.; Clark, N. A.; Hermann, A. M. *Appl. Phys. Lett.* **1991**, *59*, 1506. (c) Coleman, R. V.; Drake, B.; Hansma, P. K.; Slough, G. Phys. Rev. Lett. 1985, 55, 394-397.

[16](a) Bai, C.; Dai, C.; Zhu, C.; Chen, Z.; Huang, G.; Wu, X.; Zhu, D.; Baldeschwieler, J. D. *J. Vac. Sci. Technol. A* **1990**, *8*, 484-487. (b) Yoshimura, M.; Shigekawa, H.; Nejoh, H.; Saito, G.; Saito, Y.; Kawazu, A. *Phys. Rev. B*, **1991**, *43*, 13590-13593. (c) Bando, H.; Kashiwaya,

S.; Tokumoto, H.; Anzai, H.; Kinoshita, N.; Kajimura, H. *J. Vac. Sci. Technol.* **1990**, *A8*, 479-483. (d) Yoshimura, M.; Ara, N.; Kageshima, M.; Shiota, R.; Kawazu, A.; Shigekawa, H.; Saito, Y.; Oshima, M.; Mori, H.; Yamochi, H.; Saito, G. *Surface Science* **1991**, *242*, 18-22.

[17](a) Fainchtein, R.; Murphy, J. C. *J. Vac. Sci. Technol. B*, **1991**, *9*, 1013. (b) Pan, S.; Delozanne, A. L.; Fainchtein, R. *Journal of Vacuum Science & Technology B* **1991**, *9*, 1017-1021. (c) Li, S.; White, H. S.; Ward, M. D., preceding paper in this issue.

[18]Sleator, T.; Tycko, R. *Phys. Rev. Lett.* **1988**, *60*, 1418.

[19](a) Magonov, S. N.; Schuchhardt, J.; Kempf, S.; Keller, E.; Cantow, H.-J. *Synth. Met.* **1991**, *40*, 59-72. (b) Magonov, S. N.; Kempf, S.; Rotter, H.; Cantow, H.-J. *Synth. Met.* **1991**, *40*, 73-86.

[20](a) Blonder, G. E.; Tinkham, M. *Phys. Rev. B*, **1983**, *27*, 112. (b) van Bentum, P. J. M.; van Kempen, H.; van de Leemput, L. E. C.; Teunissen, P. A. A.; *Phys. Rev. Lett.* **1988**, *60*, 369-372.

[21](a) Nowack, A.; Weger, M.; Schweitzer, D.; Keller, H. J. *Solid State Commun.* **1986**, *60*, 199-202. (b) Hawley, M. E.; Gray, K. E.; Terris, B. D.; Wang, H. H.; Carlson, K. D.; Williams, J. M. *Phys. Rev. Lett.***1986**, *57*, 629-632. (c) Maruyama, Y.; Inabe, T.; Yamochi, H.; Saito, G. *Solid State Commun.* **1988**, *67*, 35-37. (d) Nowack, A.; Poppe, U.; Weger, M.; Schweitzer, D.; Schwenk, H. *Z. Phys. B.* **1987**, *68*, 41-47. (e) Maruyama, Y.; Hirose, R.; Saito, G.; Inokuchi, H. *Solid State Commun.* **1983**, *47*, 273-274. (f) Bando, H.; Kajimura, K.; Anzai, H.; Ishiguro, T.; Saito, G. *Proc. Seventeenth International Conference on Low-Temperature Physics*, Ecken, U.; Schmid, A.; Weber, W.; Wuhl, H., Eds.; North-Holland, Amsterdam, **1984**, p713-714. (g) More, C.; Roger, G.; Sorbier, J. P.; Jerome, D.; Ribault, M.; Bechgaard, K. *J. Phys. Lett. (Paris)* **1981**, *42*, L313-L317.

[22](a) Berlinsky, A. J.; Carolan, J. F. *Solid State Comm.* **1974**, *15*, 795 - 801. (b) Lowe, J. P. *J. Amer. Chem. Soc.* **1980**, *102*, 1262-1269.

[23]Li, S.; White, H. S.; Ward, M. D., preceding paper.

[24]An alternative explanation for the observation of two columns of tunneling current may involve tunneling into opposite ends of the TCNQ stack on the surface. In this case the *resolved* distance in the (010) plane along the [001] direction between the two ends of the molecule, chosen as the exocyclic methylidene carbon atoms, is approximately 3 Å which is much less than the 6.5 Å between STM features. Tunneling to different ends of the TCNQ molecule would require that the charge density within the TCNQ molecules in the tetramers be highly polarized, with the corresponding state density modulated along the stacks. The absence of intramolecular polarization in images of the (001) face, however, argue against this interpretation.

[25]Lee, P. A.; Rice, T. M.; Anderson, P. W. *Solid State Comm.* **1974**, *14*, 703-708.

[26](a) Torrance, J. B. *Phys. Rev. B* **1978**, *17*, 3099. (b) Kagoshima, S.; Ishiguro, T.; Schultz, T. D.; Tomkiewicz, Y. *Solid State. Comm.* **1978**, *28*, 485. (c) Abrahams, E.; Solyom, J.; Woynarovich, F. **Phys. Rev. B** *1977*, **16**, 5238.

[27](a) Kobayashi, H.; Kobayashi, A. *Extended Linear Chain Compounds*, Vol 2, **1982**, Miller, J. S., Ed.; Plenum Press, New York; p 275. (b) Friedel, J. Electron-Phonon Interactions and Phase Transitions, Vol 29, 1977; Riste, T., Ed.; Plenum Press, New York, pp. 1-49. (c) Kagoshima, S. *Extended Linear Chain Compounds*, Vol 2, **1982**, Miller, J. S., Ed.; Plenum Press, New York; p 311.

[28]$\kappa_0(x)$ is the complete elliptic integral of the first kind, which for $x>>1$, $2\kappa_0(x) \approx (p/2x)^{1/2}e^{-x}$. In this case $x = 2k_F d_{S\text{-}S}^{[hkl]}$.

[29](a) Saub, K.; Barisic, S.; Friedel, *J. Phys. Lett.* **1976**, *56A*, 302-304. (b) Heeger, A. J. in *Chemistry and Physics of One-Dimensional Metals*; Keller, H. J., Ed.; Plenum Press, New York, pp. 87-135.

[30]Oostra, S.; De Lange, P.; Visser, R. J. J. *J. Phys. C* **1983**, *44*, 1383.

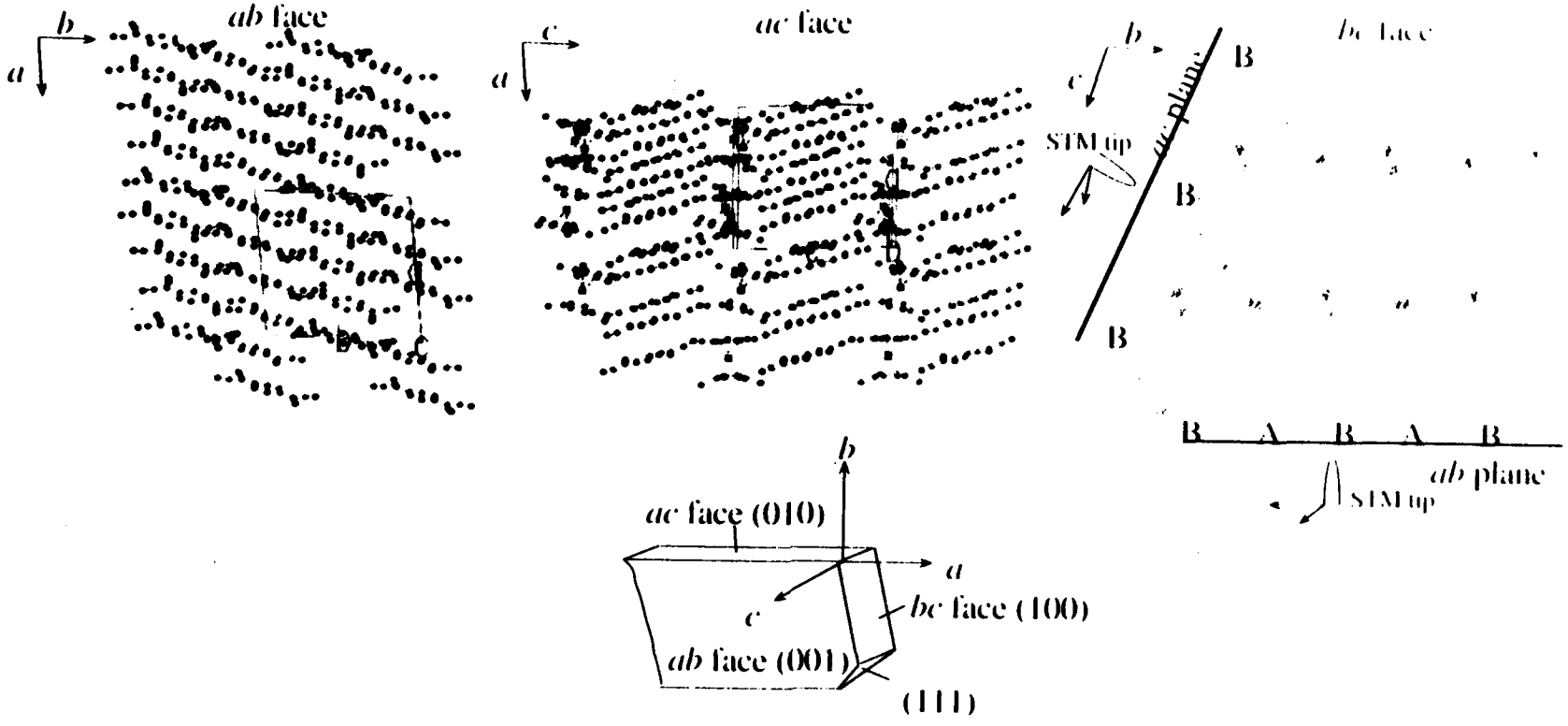
ab face
b
a
ac face
c
a
b
c
STM tip
ac plane
B
B
B
bc face
B A B A B
ab plane
STM tip
b
ac face (010)
a
c
bc face (100)
ab face (001)
(111)

3.29 3.29 3.24 3.24

Stack B

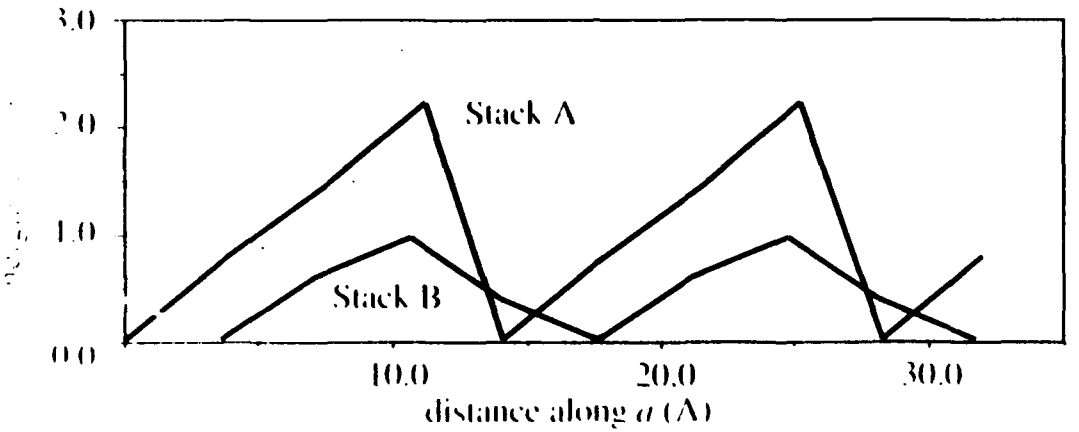

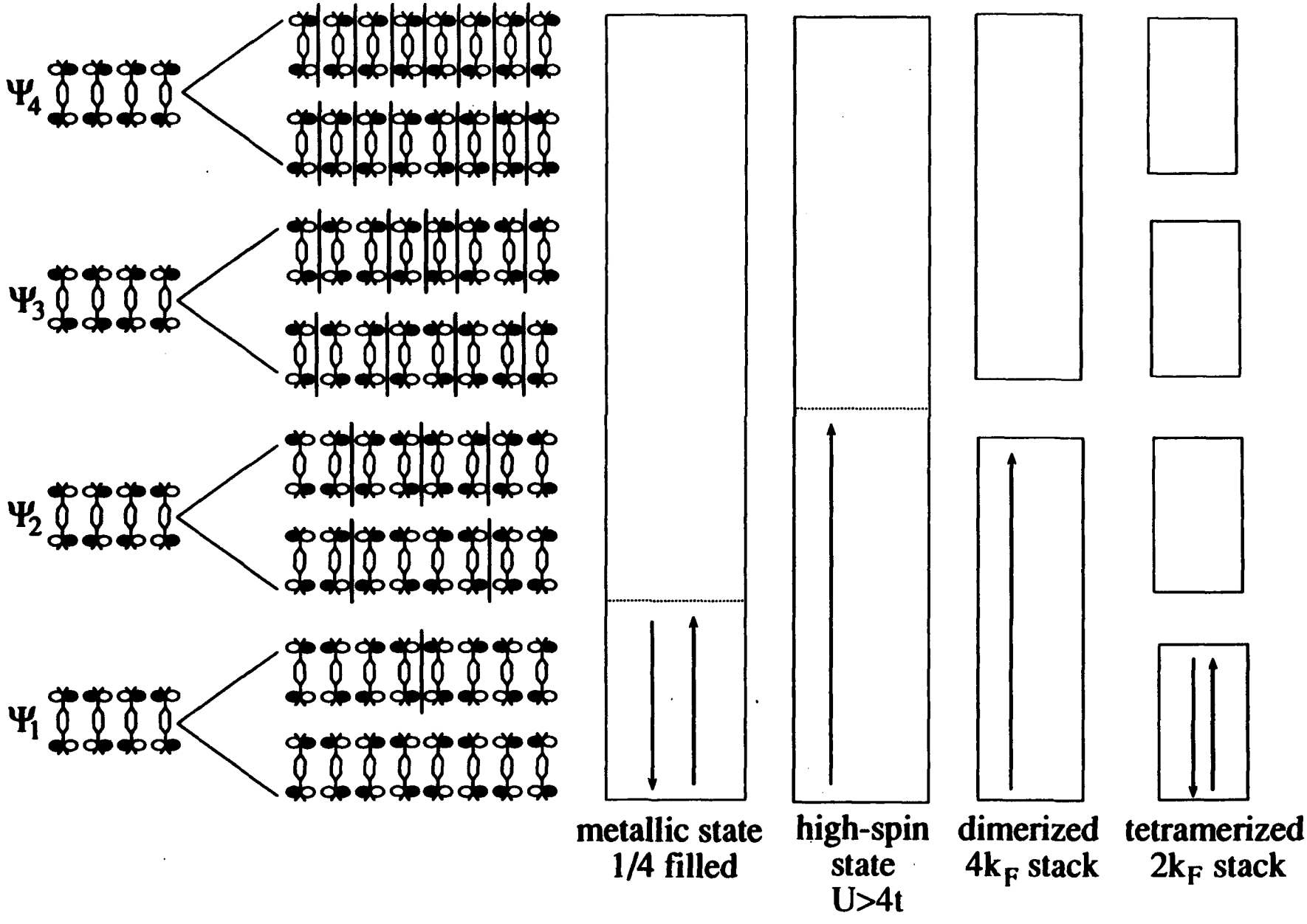
Ψ_4
Ψ_3
Ψ_2
Ψ_1
metallic state
1/4 filled
high-spin
state
U>4t
dimerized
$4k_F$ stack
tetramerized
$2k_F$ stack

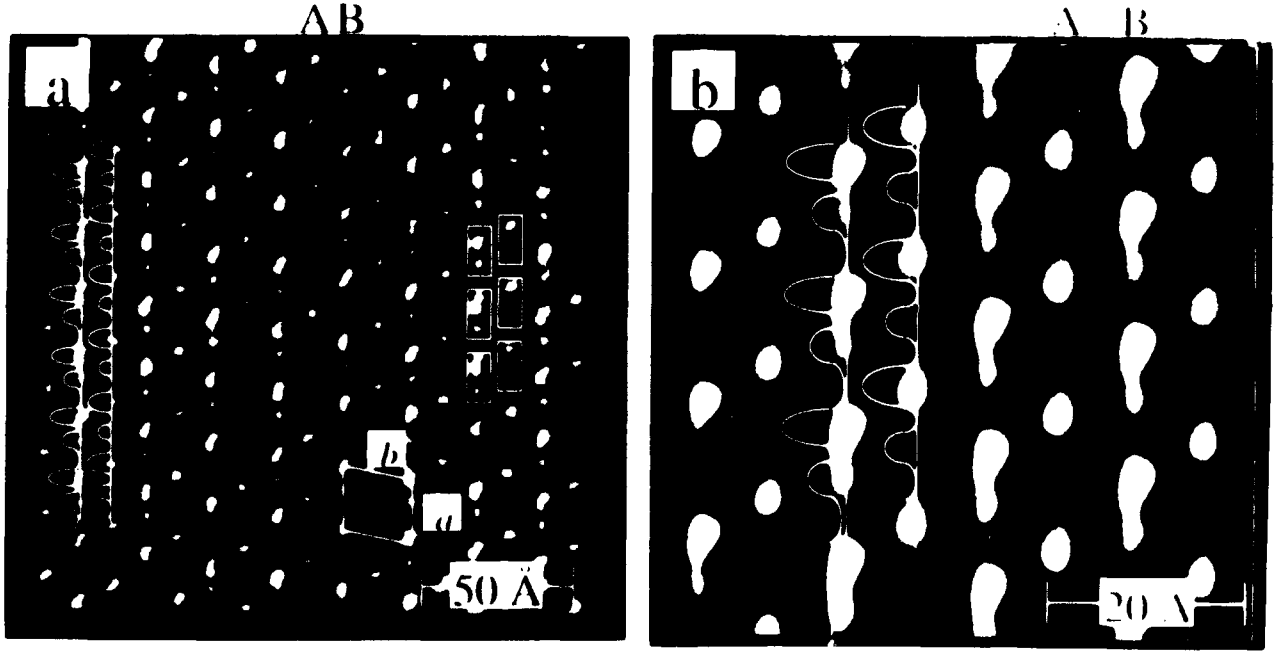
A B
a
b
a
50 Å
A B
b
20 Å

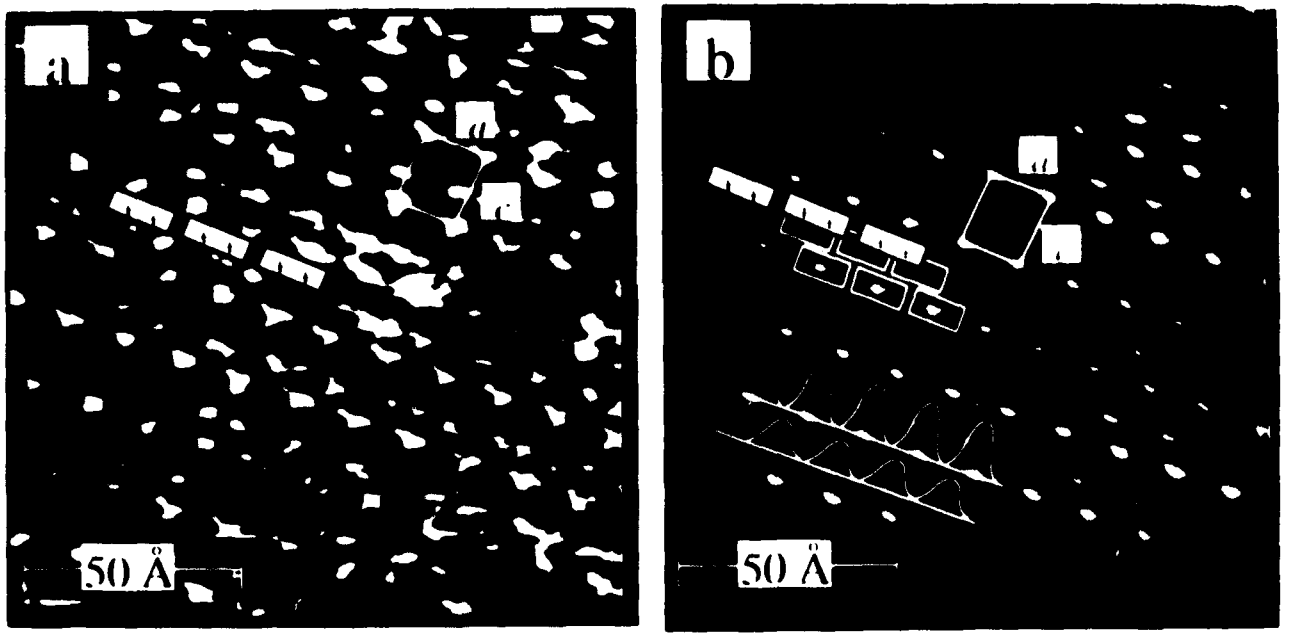
a
50 Å
b
50 Å

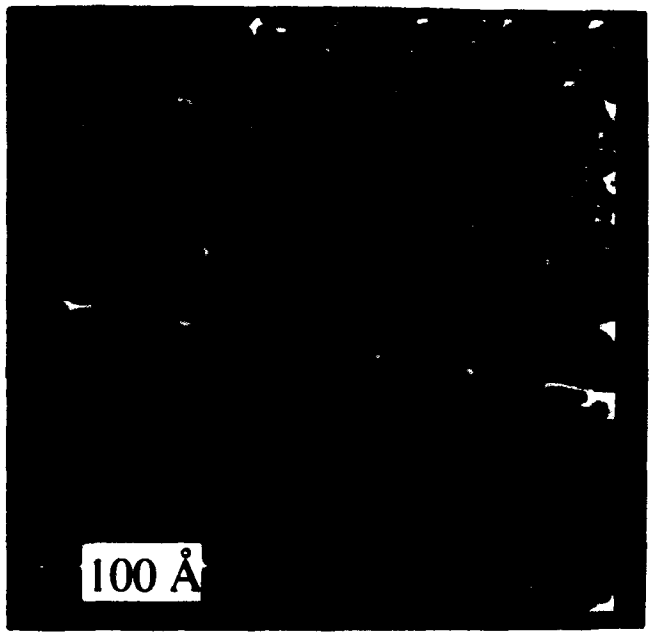
100 Å

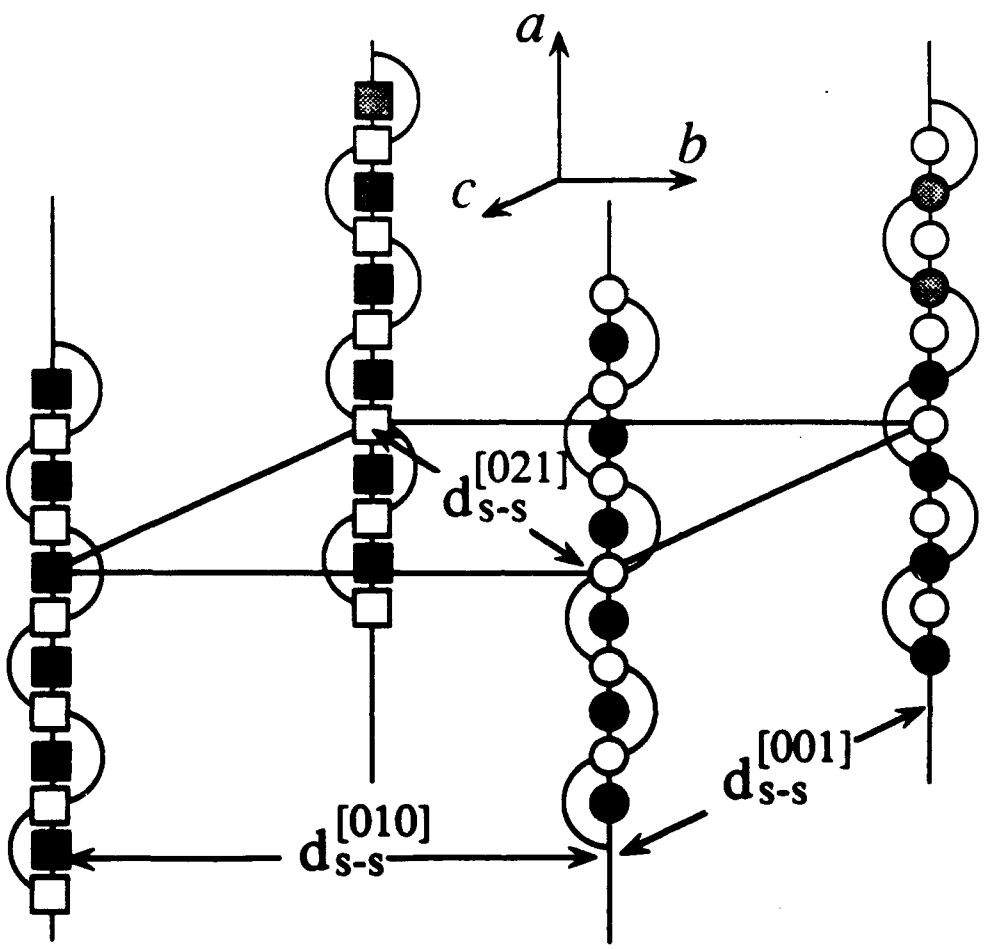
a
b
c
$d^{[021]}_{s\text{-}s}$
$d^{[001]}_{s\text{-}s}$
$d^{[010]}_{s\text{-}s}$